and CF_4. The values of $D_{AB}(-1)$ for the C-H bonds highlight the much lower reactivity of CHF_3 toward the hydroxyl radical.

In the cases considered here, the need to rotate one molecule relative to another did not arise. However, it should be stressed that this is very straightforward, and the ability to do this has already been implemented in our programs. We have not, as yet, considered distortion of the molecule(s) by means of, e.g., rotations about individual bonds.

The ability to use semiempirical wave functions and also to concentrate on particular regions of a molecular system means that it is now possible to compute values of $D_{AB}(n)$ for large series of large molecules. It is also possible to compare different regions of the same molecule. Comparisons of HOMOs and/or LUMOs could also be worthwhile. No single measure of similarity can be expected to be a universal panacea, but we believe that the momentum-space indices described here are likely to prove useful in structure-activity relations, particularly those involving binding energies to biologically active systems.

Registry No. CH_3OCH_3, 115-10-6; CH_3SCH_3, 75-18-3; $CH_3CH_2CH_3$, 74-98-6; CH_3F, 593-53-3; CH_2F_2, 75-10-5; CHF_3, 75-46-7; CF_4, 75-73-0; CH_4, 74-82-8.

Stereochemically Active or Inactive Lone Pair Electrons in Some Six-Coordinate, Group 15 Halides

Ralph A. Wheeler* and P. N. V. Pavan Kumar†

Contribution from the Department of Chemistry and Biochemistry, 620 Parrington Oval, Room 208, University of Oklahoma, Norman, Oklahoma 73019. *Received October 21, 1991*

Abstract: The valence shell electron pair repulsion (VSEPR) model has enjoyed remarkable success explaining the shapes of molecules consisting of main group atoms. Exceptional compounds are known, however, which display the "inert pair effect": they contain a lone pair of electrons that appear spherically symmetrical and are thus stereochemically inactive. We consider BiI_6^{3-}, $BiCl_6^{3-}$, BiI_3, and SbI_3 as prototypical molecules and solids containing six-coordinate, group 15 atoms with stereochemically active or inactive lone pair electrons on the central atom. Extended Hückel molecular orbital and crystal orbital calculations show an underlying tendency for a second-order Jahn-Teller distortion from octahedral to trigonal coordination of the central atom. The distortion mixes the central atom p_z character of the unoccupied orbitals with the s character of the HOMO and thus hybridizes the lone pair electrons toward the longer M-X bonds (M = Bi or Sb; X = I or Cl). For the MX_3 compounds, the hybrid lone pair points toward the *smaller* X-M-X angles, and the basic assumption of the VSEPR model is confounded for extended solids. Whether or not the distortion is structurally realized for the BiI_6^{3-} and $BiCl_6^{3-}$ molecules depends upon the balance between HOMO-LUMO mixing and (1) the mixing between the HOMO and a lower energy $1a_1$ orbital with ligand lone pair and Bi p_z character and (2) repulsions among ligand lone pairs. The HOMO-$1a_1$ mixing is strongest and ligand lone pair-lone pair repulsions are greatest for large, electropositive ligands. HOMO-LUMO mixing predominates for the compounds that display trigonal distortions ($BiCl_6^{3-}$ and SbI_3), but not for those that remain octahedral (BiI_6^{3-} and BiI_3).

Introduction

Compounds containing six-coordinate main group elements are remarkable for the variety of coordination geometries observed. Several striking examples are the isoelectronic molecules BiI_6^{3-} (**1**)[2h] and $BiCl_6^{3-}$ (**2**)[2a-g] as well as the extended solids BiI_3 (**3**) and SbI_3.[3a] Each pair of compounds (BiI_6^{3-} and $BiCl_6^{3-}$; BiI_3 and SbI_3) is extraordinary because both structures of the pair cannot be explained by simple models such as valence shell electron pair repulsion (VSEPR).[4] In particular, lone pair electrons on the central Bi atoms of BiI_6^{3-} and BiI_3 are not evident in the structures. They are stereochemically inactive and give rise to what has been called the "inert pair" effect.[4] We will develop these ideas more fully later, after discussing the structures shown in **1-3** and after introducing a number of compounds with similar structures. Then we will present a simple, unified model based

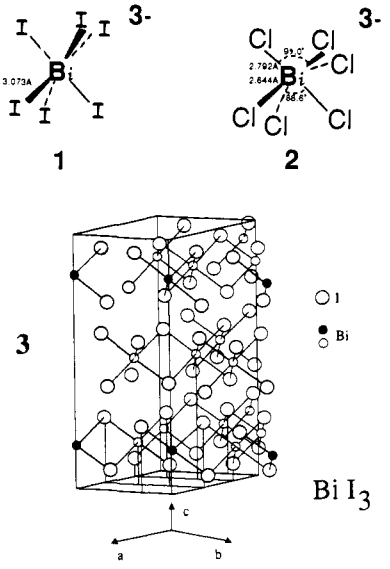

† Current address: Department of Chemistry, University of Texas at Arlington, Arlington, TX 76019-0065.

(1) General reference for MX_6^{n-} and MX_n (M = group 13-18 central atom, X = halogens): Wells, A. F. *Structural Inorganic Chemistry*, 5th ed.; Clarendon Press: Oxford, 1984.

(2) $BiCl_6^{3-}$: (a) Morss, L. R.; Robinson, W. R. *Acta Crystallogr.* **1972**, 28 B, 653-654. (b) Lazarini, F. *Acta Crystallogr.* **1987**, *43C*, 637-638. (c) Battaglia, L. P.; Corradi, A. B.; Nardelli, M.; Tani, M. E. V. *J. Chem. Soc., Dalton Trans.* **1978**, 583-587. (d) Atoji, M.; Watanabe, T. *J. Chem. Phys.* **1952**, *20*, 1045-1046. (e) du Bois, A.; Abriel, W. *Z. Naturforsch.* **1988**, *43B*, 1003-1009. (f) du Bois, A.; Abriel, W. *Z. Kristallogr.* **1988**, *182*, 36-38. (g) Benachenhou, F.; Mairesse, G.; Nowogrocki, G.; Thomas, D. *J. Solid State Chem.* **1986**, *65*, 13-26. (h) BiI_6^{3-}: Lazarini, F. *Acta Crystallogr.* **1977**, *33B*, 1957-1959.

(3) BiI_3: (a) Trotter, J.; Zobel, T. *Z. Kristallogr.* **1966**, *123*, 67-72. (b) Davidovich, R. L.; Buslaev, Y. A. *Koord. Khim.* **1988**, *14*, 1011-1036. (c) Pearson, W. B. *The Crystal Chemistry and Physics of Metals and Alloys*; Wiley: New York, 1972; p 445. (d) Greenwood, N. N.; Earnshaw, A. *Chemistry of Elements*; Pergamon Press: Oxford, 1984; p 652.

(4) VSEPR: (a) Gillespie, R. J.; Nyholm, R. S. *Quart. Rev. Chem. Soc.* **1957**, *11*, 339. (b) Searcy, A. W. *J. Chem. Phys.* **1958**, *28*, 1237-1242. (c) Gillespie, R. J. *J. Am. Chem. Soc.* **1960**, *82*, 5978-5983. (d) Gillespie, R. J. *J. Chem. Educ.* **1963**, *40*, 295-301; *Ibid.* **1970**, *47*, 18-23. (e) Gillespie, R. J. *Molecular Geometry*; Van Nostrand and Reinhold: London, 1972. (f) Huheey, J. E. *Inorganic Chemistry, 3rd ed.*; Harper and Row: New York, 1983; p 208. (g) Jolly, W. L. *Modern Inorganic Chemistry, 2nd ed.*; McGraw-Hill: New York, 1991.

0002-7863/92/1514-4776$03.00/0

on extended Hückel molecular orbital calculations for understanding the structures of the molecular (BiI_6^{3-} and $BiCl_6^{3-}$) and solid-state (BiI_3 and SbI_3) compounds.

Six-Coordinate Main Group Halides

Halides with six-coordinate group 15 atoms adopt several different geometries. The most common structures are exemplified by BiI_6^{3-} (**1**) and $BiCl_6^{3-}$ (**2**). The central Bi atom of **1** is octahedrally coordinated by six iodines at a distance of 3.073 Å,[1] whereas **2** exists in two forms, one with regular octahedral coordination of Bi[2a] and another with a trigonal distortion from the symmetrical octahedral geometry.[2e,f] The trigonal distortion gives $BiCl_6^{3-}$ approximate C_{3v} symmetry, with three Bi–Cl bond lengths of 2.644 Å and three Bi–Cl distances of 2.792 Å. Similarly, the two sets of nominally different Cl–Bi–Cl angles marked in **2** show three larger (91.0°) and three smaller (88.6°) values. If we assign each halide ligand a 1– charge, both **1** and **2** acquire a 3– charge if Bi is assigned a 3+ formal oxidation state. Since Bi is a group 15 element with five valence electrons, Bi^{3+} should have a lone pair of electrons in both **1** and **2**.

The solid-state compounds BiI_3 (**3**) and SbI_3 show a relationship to one another similar to the relationship between BiI_6^{3-} and $BiCl_6^{3-}$. BiI_3 consists of a hexagonal close-packed lattice of iodines, with 6^3 nets of Bi atoms between alternate pairs of iodine layers.[3] Thus, the Bi atoms fill two-thirds of the octahedral holes between adjacent iodine layers, or one-third of the octahedral holes in the entire structure. **4** shows a projection of the BiI_3 structure, viewed

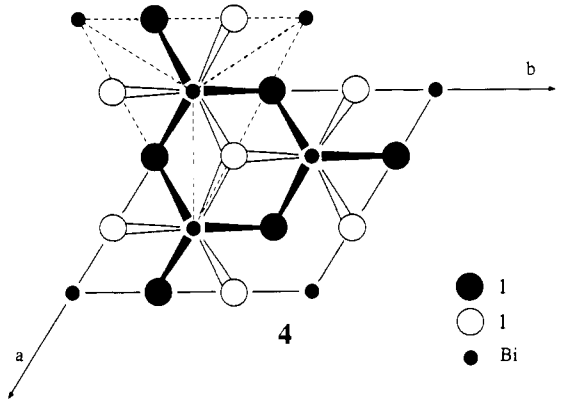

4

down the hexagonal *c* axis, to highlight the octahedral coordination of Bi by six iodines, 3.07 Å away. The dashed lines in **4** outline the rhombohedral unit cell used in the extended Hückel band calculations. The structure of SbI_3 is similar to **3** except that the Sb atoms are displaced by 0.320 Å along the hexagonal *c* axis. This results in a distortion from octahedral coordination, similar to that observed in $BiCl_6^{3-}$ (**2**) and resulting in three short (2.87 Å) and three long (3.32 Å) Sb–I distances in SbI_3.[3a] Like the molecular compounds described earlier, BiI_3 and SbI_3 contain Bi^{3+} and Sb^{3+}, each with a lone pair of electrons. Like the lone pairs on Bi in the BiI_6^{3-} molecule, the Bi lone pairs in the solid-state compound BiI_3 are stereochemically inactive, inert pairs.

The compounds just described, i.e., BiI_6^{3-}, $BiCl_6^{3-}$, BiI_3, and SbI_3, are not unique. Indeed, there are far too many related structures for us to consider them all, but Tables I and II list representative examples. Table I lists a number of structurally well-characterized main group halides of the type MX_6^{n-}, with octahedral or distorted octahedral coordination of the central atom, M.[5-20,52] The most prominent structural trends displayed by the compounds in Table I appear for group 15; they include a tendency for octahedral coordination for highly electropositive central atoms

Table I. Geometric Parameters for MX_6^{n-}[a]

M	X = F	X = Cl	X = Br	X = I
Sn[5,7a]		2.763, 2.894	3.080	
		95.9, 84.3	90.0	
Pb[6-9]		2.885	3.130	3.217
		90.0	90.0	90.0
Sb[10,11]		2.415, 3.114	2.622, 3.061	
		90.4, 81.7	92.2, 90.7	
		2.652	2.794	
		90.9	90.9	
Bi[1,2,12]		2.660	2.849	3.073
		90.0	92.5	90.0
		2.644, 2.792	2.749, 3.006	
		91.0, 88.6	92.8, 89.6	
Se[13,14]		2.402	2.577	
		90.0	90.0	
			2.547, 2.595	
			92.6, 90.1	
Te[15-17]		2.538	2.694	2.934
		90.0	90.0	90.0
		2.460, 2.610	2.580, 2.840	
		90.6, 88.3	91.0, 94.6	
Br[18]	1.854			
	90.0			
Xe[20]	1.89			

[a] M = central main group atom, X = halogen; n = 0–4. From published results of diffraction experiments. For each compound, numbers in the first row refer to the M–X distances (Å) and numbers in the second row correspond to the X–M–X angle (deg). Superscripts on M refer to the literature references.

(5) $SnCl_6^{4-}$: Kimura, T.; Sakurai, T. *J. Solid State Chem.* **1980**, *34*, 369–376.

(6) PbF_6^{4-}: S.-Dumont, O.; Bergerhoff, G.; Hartert, E. *Z. Anorg. Allg. Chem.* **1956**, *283*, 314–329.

(7) $PbCl_6^{4-}$: (a) Andrews, R. H.; Clark, S. J.; Donaldson, J. D.; Dewan, J. C.; Silver, J. *J. Chem. Soc., Dalton Trans.* **1983**, 767–770. (b) Petrov, V. V.; Bogdanova, A. V.; Vagina, M. A.; Zavodnik, V. E.; Gladyshevskii, E. I.; Pecharskii, V. K.; Mokraya, I. R. *Sov. Phys. Crystallogr.* **1987**, *32*, 289–290.

(8) $PbBr_6^{4-}$: Beck, H. P.; Milius, W. *Z. Anorg. Allg. Chem.* **1988**, *562*, 102–104.

(9) PbI_6^{4-}: (a) Vincent, B. R.; Robertson, K. N.; Cameron, T. S.; Knop, O. *Can. J. Chem.* **1987**, *65*, 1042–1046. (b) Moller, C. K. *Mat.-Fys. Medd.-K. Dan. Vldensk. Selsk.* **1960**, *32*, Nos. 1 and 2.

(10) $SbCl_6^{3-}$: (a) Vezzosi, I. M.; Battaglia, L. P.; Corradi, A. B. *Inorg. Chim. Acta* **1984**, *89*, 151–155. (b) Schroeder, D. R.; Jacobson, R. A. *Inorg. Chem.* **1973**, *12*, 210–213. (c) Knodler, F.; Ensinger, U.; Schwarz, W.; Scmidt, A. *Z. Anorg. Allg. Chem.* **1988**, *557*, 208–218. (d) Lawton, S. L.; Jacobson, R. A. *Inorg. Chem.* **1966**, *5*, 743–749. (e) Prassides, K.; Day, P.; Cheetam, A. K. *J. Am. Chem. Soc.* **1983**, *105*, 3366–3368. (f) Prassides, K.; Day, P.; Cheetam, A. K. *Inorg. Chem.* **1985**, *24*, 545–552.

(11) $SbBr_6^{3-}$: Okuda, T.; Hiura, M.; Koshimizu, E.; Ishihara, H.; Kushi, Y.; Negita, H. *Chem. Letts.* **1982**, 1321–1324.

(12) $BiBr_6^{3-}$: (a) McPherson, W. G.; Meyers, E. A. *J. Phys. Chem.* **1968**, *72*, 3117–3122. (b) Lazarini, F. *Acta Crystallogr.* **1978**, *34B*, 2288–2290. (c) Lazarini, F. *Acta Crystallogr.* **1985**, *41C*, 1617–1619. (d) Lazarini, F. *Acta Crystallogr.* **1980**, *36B*, 2748–2750.

(13) $SeCl_6^{2-}$: Abriel, W. *Acta Crystallogr.* **1986**, *42C*, 1113–1115.

(14) $SeBr_6^{2-}$: Abriel, W. *Z. Naturforsch.* **1987**, *42B*, 415–420.

(15) $TeCl_6^{2-}$: (a) du Bois, A.; Abriel, W. *Z. Naturforsch.* **1990**, *45B*, 573–578. (b) Abriel, W.; Friedrich, C. *Z. Naturforsch.* **1985**, *40B*, 1691–1697. (c) Abriel, W. *Z. Naturforsch.* **1986**, *41B*, 592–598. (d) du Bois, A.; Abriel, W. *Acta Crystallogr.* **1989**, *45C*, 1986–1988. (e) Abriel, W. *Acta Crystallogr.* **1986**, *42B*, 449–453. (f) Ghozlen, M. H. B.; Bats, J. W. *Acta Crystallogr.* **1982**, *38B*, 1308–1309. (g) Hinrichs, W.; Mandak, D.; Klar, G. *Cryst. Struct. Comm.* **1982**, *11*, 309–314. (h) Michelet, A.; Toffoli, P.; Rodier, N. *Acta Crystallogr.* **1986**, *42C*, 413–415. (i) Milne, J.; Philippot, E.; Maurin, M. *Rev. Chim. Miner.* **1984**, *21*, 749. (j) Ault, H. K.; Husebye, S. *Acta Chem. Scand.* **1978**, *32A*, 157–162. (k) Rosso, U.; Calogero, S.; Valle, G. *Cryst. Struct. Commun.* **1980**, *9*, 829–834. (l) Rosso, U.; Valle, G.; Calogero, S. *J. Chem. Soc. Dalton Trans.* **1980**, 2303–2305.

(16) $TeBr_6^{2-}$: (a) Abrahams, S. C.; Ihringer, J.; Marsh, P. *Z. Kristallogr.* **1989**, *186*, 1–2. (b) Abriel, W. *Z. Kristallogr.* **1983**, *162*, 2–4. (c) Abriel, W. Zehnder, E.-J. *Z. Naturforsch.* **1987**, *42B*, 1273–1281. (d) Abriel, W. *Z. Naturforsch.* **1983**, *38B*, 1543–1547. (e) Abrahams, S. C.; Ihringer, J.; Marsh, P. *Acta Crystallogr.* **1989**, *45B*, 26–34. (f) Abriel, W.; Ehrhardt, H. *Angew. Chem., Int. Ed. Engl.* **1984**, *23*, 963–965. (g) Abriel, W.; du Bois, A. *Acta Crystallogr.* **1989**, *45C*, 2002–2003. (h) Abriel, W.; Ihringer, J. *J. Solid State Chem.* **1984**, *52*, 274–280. (i) Dahan, F.; L.-Soubeyran, O. *Acta Crystallogr.* **1976**, *32B*, 2859–2862. (j) Brown, I. D. *Can. J. Chem.* **1964**, *42*, 2758–2767. (k) Dahan, F.; L.-Soubeyran, O. *Acta Crystallogr.* **1976**, *32B*, 2863–2866. (l) Kumar, V.; Aravamudan, G.; Seshasayee, M. *Polyhedron* **1990**, *9*, 2879–2885. (m) Krebs, B.; Bonmann, S.; Erpenstein, K. *Z. Naturforsch.* **1991**, *46B*, 919–930.

(17) TeI_6^{2-}: (a) Abriel, W.; du Bois, A. *Z. Naturforsch.* **1989**, *44B*, 1187–1194. (b) Kiriyama, H.; Mizuhashi, Y.; Ootani, J. *Bull. Chem. Soc. Jpn.* **1986**, *59*, 581–585. (c) Abriel, W. *Mat. Res. Bull.* **1982**, *17*, 1341. (d) L'Haridon, P.; Jedrzejczak, H.; Szwabski, S. *Acta Crystallogr.* **1979**, *35B*, 1843–1846.

(18) BrF_6^-: Mahjoub, A. R.; Hoser, A.; Fuchs, J.; Seppelt, K. *Angew. Chem., Int. Ed. Engl.* **1989**, *28*, 1526–1527.

Table II. Structural Parameters for MX_n[a]

M	X = F	X = Cl	X = Br	X = I
Ge[21-23]	1.79, 2.57	2.18[b]	2.60, 3.37	
	92.0, 85.0	100.3	90.4, 85.8	
N[24,25]	1.37[b]	1.75, 3.68		
	102.5	106.8, 102.6		
P[26-29]	1.57[b]	2.04[b]	2.20[b]	2.43[b]
	97.8	100.3	101.0	102.0
				2.46, 3.67
				102.0, 89.4
As[30-33]	1.71[b]	2.16[c]	2.32[b]	2.55[b]
	96.2	98.7	99.7	100.2
				2.59, 3.47
				99.7, 96.0
Sb[34-37]	1.92, 2.61	2.33[b]	2.49[b]	2.72[b]
	88.9, 106.1	97.2	98.2	99.1
			2.5	2.87, 3.32
			95.5	99.0, 95.8
			2.49	
			95.1	
Bi[38,39]			2.66, 3.32	3.1
			96.3, 88.2	90.0
		2.48[b]	2.82	
		100.0	90.0	
			2.63[b]	
			100.0	
S[40]	1.54, 1.64[c]			
	103.8			
Se[41-43]	1.68, 1.77[c]	2.16, 2.86	2.37, 2.98	
	100.6	95.8, 83.1	95.4, 86.4	
Te[44-46]	1.92, 2.26	2.31, 2.93		2.77, 3.11, 3.23
	86.5	94.8, 85.1		94.6, 86.0, 84.9
Cl[47]	1.57, 1.67			
	86.0			
	1.58, 1.67[c]			
	86.0			
Br[48]	1.71, 1.81			
	85.4, 80.6			
	1.77, 1.67[b]			
	85.9			
I[49]	1.75, 1.87			
	81.9			
	1.86, 1.85[b]			
	82.6			

[a] M = central main group atom, X = halogen; n = 2-6. For each compound, numbers in the first row refer to the M-X distances (Å) and numbers in the second row correspond to the X-M-X angle (deg). Superscripts on M refer to the literature references. [b] Electron diffraction data. [c] Microwave data.

and large, electropositive ligands. Thus, BiI_6^{3-} (1) contains octahedrally coordinated Bi, but the other compounds containing smaller ligands or less electronegative central atoms, i.e., $BiBr_6^{3-}$, $BiCl_6^{3-}$, $SbBr_6^{3-}$, and $SbCl_6^{3-}$, each show two structures, one with octahedral and another with approximate C_{3v} symmetry about the central atom.

Table II lists structural parameters for neutral main group halides with the empirical formula MX_n from groups 14-17. Some of the compounds listed are extended solids related to BiI_3, but a number of them are molecular structures.[21-52] We have already seen that 3 is an extended solid containing octahedrally coordinated Bi. In contrast, the extended solid $BiBr_3$ shows two different

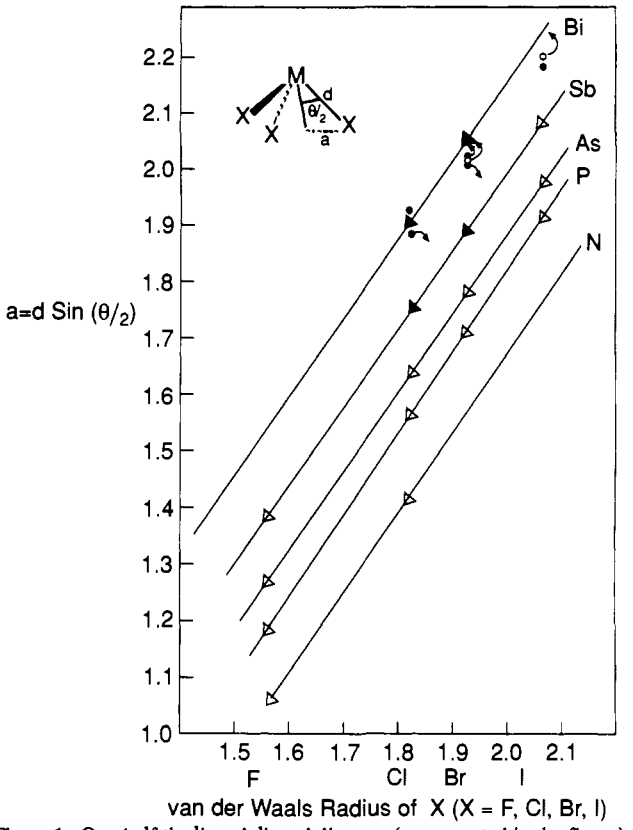

Figure 1. One-half the ligand-ligand distance (as computed in the figure) vs the van der Waals radius of the ligand X (X = F, Cl, Br, or I) using the data from MX_6^{3-} and MX_3 (M = N, P, As, Sb, or Bi) shows a linear correlation. △ and ▲ refer to trigonally distorted structures of MX_3 and MX_6^{3-}, respectively. Similarly, ○ and ● refer to the octahedral structures of MX_3 and MX_6^{3-}.

(19) IF_6^-: (a) Christie, K. O.; Guertin, J. P.; Sawodny, W. *Inorg. Chem.* **1968**, *7*, 626-628. (b) Christie, K. O.; Wilson, W. W. *Inorg. Chem.* **1989**, *28*, 3275-3277.

(20) XeF_6: (a) Gillespie, R. J. In *Noble Gas Compounds*; Hyman, H. H., Ed.; Univ. Chicago Press: Chicago, 1963; p 333. (b) Bartell, L. S.; Gavin, R. M., Jr.; Thomson, H. B.; Chernick, C. L. *J. Chem. Phys.* **1965**, *43*, 2547-2548. (c) Gavin, R. M., Jr.; Bartell, L. S. *J. Chem. Phys.* **1968**, *48*, 2460-2465; 2466-2483. (d) Greenwood, N. N.; Earnshaw, A. E. *Chemistry of the Elements*; Pergamon Press: Oxford, 1984; p 1048. (e) Herndon, W. C. *J. Mol. Struct. (THEOCHEM)* **1988**, *169*, 389-401. (f) Bartell, L. S. *J. Chem. Phys.* **1967**, *46*, 4530-4531. (g) Huheey, J. E. *Inorganic Chemistry*; Harper and Row: New York, 1983; p 216.

(21) GeF_2: Trotter, J.; Akhtar, M.; Bartlett, N. *J. Chem. Soc. A* **1966**, 30-33.

(22) $GeCl_2$: Schultz, G.; Tremmel, J.; Hargittai, I.; Berecz, I.; Bohatka, S.; Kagramanov, N. D.; Maltsev, A. K.; Nefedov, O. M. *J. Mol. Struct.* **1979**, *55*, 207-214.

(23) $GeBr_2$: Rouse, R. C.; Peacor, D.; Maxim, B. R. *Z. Kristallogr.* **1977**, *145*, 161-171.

(24) NF_3: (a) General Structural data on MX_3: Galy, J.; Enjalbert, R. *J. Solid State Chem.* **1982**, *44*, 1-23. (b) Passmore, J.; Richardson, E. K.; Whidden, T. K.; White, P. S. *Can. J. Chem.* **1980**, *58*, 851-857. (c) Sawyer, J. F.; Gillespie, R. J. *Prog. Inorg. Chem.* **1986**, *34*, 65-113. (d) Schomaker, V.; Lu, C.-S. *J. Am. Chem. Soc.* **1950**, *72*, 1182-1185.

(25) NCl_3: (a) Hartl, H.; Schoner, J.; Jander, J.; Schultz, H. *Z. Anorg. Allg. Chem.* **1975**, *413*, 61-71. (b) Burgi, H. B.; Stedman, D.; Bartell, L. S. *J. Mol. Struct.* **1971**, *10*, 31-38.

(26) PF_3: Morino, Y.; Kuchitsu, K.; Moritani, T. *Inorg. Chem.* **1969**, *8*, 867-871.

(27) PCl_3: (a) Hedberg, K.; Iwasaki, M. *J. Chem. Phys.* **1962**, *36*, 589-593. (c) Cazzoli, G. *J. Mol. Spectrosc.* **1974**, *53*, 37-44.

(28) PBr_3: Kuchitsu, K.; Shibata, T.; Yokozeki, A.; Matsumura, C. *Inorg. Chem.* **1971**, *10*, 2584-2587.

(29) PI_3: (a) Allen, P. W.; Sutton, L. E. *Acta Crystallogr.* **1950**, *3*, 46-72. (b) Lance, E. T.; Haschke, J. M.; Peacor, D. R. *Inorg. Chem.* **1976**, *15*, 780-781.

(30) AsF_3: (a) Konaka, S.; Kimura, M. *Bull. Chem. Soc. Jpn.* **1970**, *43*, 1693-1703. (b) Clippard, F. B., Jr.; Bartell, L. S. *Inorg. Chem.* **1970**, *9*, 805-811.

(31) $AsCl_3$: Konaka, S. *Bull. Chem. Soc. Jpn.* **1970**, *43*, 3107-3115.

(32) $AsBr_3$: (a) Samdal, S.; Barnhart, D. M.; Hedberg, K. *J. Mol. Struct.* **1976**, *35*, 67-80. (b) Robiette, A. G. *J. Mol. Struct.* **1976**, *35*, 81-84. (c) Singh, A. K.; Swaminathan, S. *Z. Kristallogr.* **1967**, *124*, 375-377. (d) Trotter, J. *Z. Kristallogr.* **1965**, *122*, 230-236.

(33) AsI_3: (a) Morino, Y.; Ukaji, T.; Ito, T. *Bull. Chem. Soc. Jpn.* **1966**, *39*, 71-78. (b) Enjalbert, R.; Galy, J. *Acta Crystallogr.* **1980**, *36B*, 914-916.

(34) SbF_3: (a) Edwards, A. J. *J. Chem. Soc. A* **1970**, 2751-2753. (b) Matsumura, C.; Takeo, H. Symposium on Molecular Structure; Oct 15, 1969.

(35) $SbCl_3$: Konaka, S.; Kimura, M. *Bull. Chem. Soc. Jpn.* **1973**, *46*, 404-407.

(36) $SbBr_3$: (a) Konaka, S.; Kimura, M. *Bull. Chem. Soc. Jpn.* **1973**, *46*, 413-416. (b) Cushen, D. W.; Hulme, R. *J. Chem. Soc.* **1964**, 4162-4166. (g) Cushen, D. W.; Hulme, R. *J. Chem. Soc.* **1962**, 2218-2222.

(37) SbI_3: (a) Almenningen, A.; Bjorvatten, T. *Acta Chem. Scand.* **1963**, *17*, 2573-2574. (b) Pohl, S.; Saak, W. *Z. Kristallogr.* **1984**, *169*, 177-184.

structures, one with octahedrally coordinated Bi and one with C_{3v} site symmetry at the Bi atom.[39] SbI_3, AsI_3, and PI_3 also display C_{3v} site symmetry, with three short and three long M–I distances, whereas the bromides, chlorides, and fluorides of these elements are molecular compounds with the central atom bonded to three halide ligands. A second, more distant coordination shell of five ligands completes the coordination geometry for the bromides, chlorides, and fluorides of Sb, As, and P. So octahedral coordination is more prevalent for compounds of the type MX_3 with electropositive, group 15 central atoms and large, electropositive ligands. As the central atom becomes more electronegative or the ligands become smaller and more electronegative, the coordination geometry usually distorts to C_{3v} geometry, until the limiting distortion of ligand dissociation is attained.

Clearly the variety of structures for the compounds listed in Tables I and II will not be easily rationalized. Several possible explanations, ranging in sophistication from VSEPR to relativistic molecular orbital calculations, have been put forth for various observed structures.[10a,15e,53,54] Although we have seen that VSEPR, with its requirement that lone pair electrons demand angular space around a central atom, cannot explain the variety of observed structures, neither is it necessary to invoke relativity

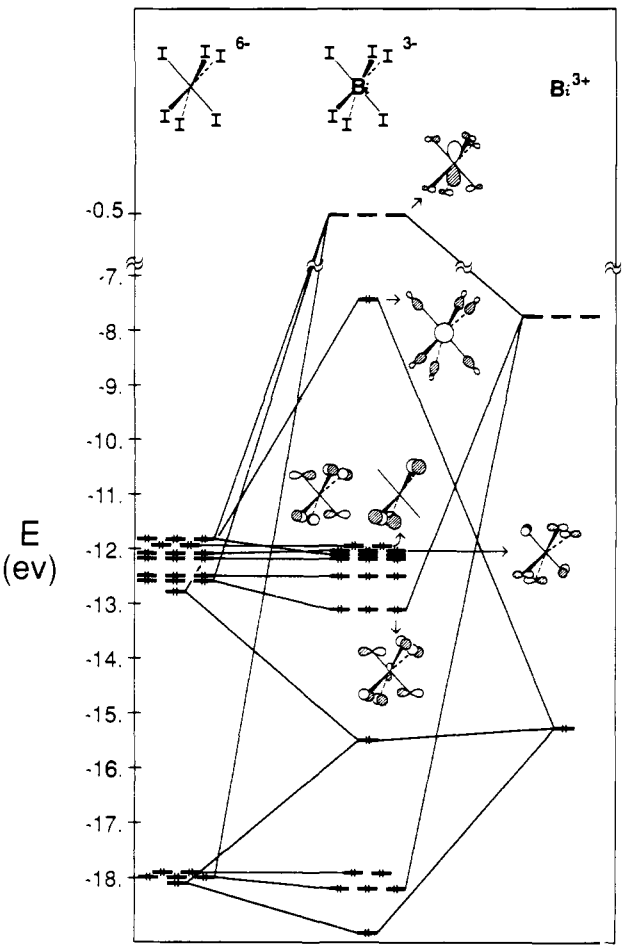

Figure 2. Interaction diagram showing how the orbitals of I_6^{6-} (left side) and Bi^{3+} (right side) interact to give the orbitals of BiI_6^{3-} (middle).

to understand structural trends. In fact Figure 1, a plot of one-half the ligand–ligand distance vs the ligand's van der Waals radius for MX_3 and MX_6^{3-} structures (M = a group 15 atom, X = a halide), implies that the assumption of ligand–ligand repulsion central to VSEPR successfully predicts ligand–ligand distances for most such compounds. If the ligands were hard spheres, we would expect Figure 1 to display a straight line with a slope of 1, passing through the origin. The plot instead shows a series of straight lines, one for each M, but nonetheless implies that for nonoctahedral structures the ligand–ligand distance is fixed by repulsions between the ligands. Since it is the octahedral structures which deviate from the correlation, one may infer that other factors, perhaps electronic effects, are responsible for the octahedral geometries. Our strategy is to search for those electronic effects by comparing MOs for the MX_6^{n-} molecules, BiI_6^{3-} and $BiCl_6^{3-}$, using the semiempirical extended Hückel method.[55] Walsh diagrams are presented to show orbital energy changes from octahedral to C_{3v} geometries. We expect orbital interactions similar to those seen in the molecular case to be important in determining structures of the solid-state compounds of the type MX_n. Bonding in the solid-state MX_3-type compounds, BiI_3 and SbI_3, is analyzed using density of states and band structure plots. Thus, we present a unified picture of the orbital reasons for the

(38) $BiCl_3$: Skinner, H. A.; Sutton, L. E. *Trans. Faraday Soc.* **1940**, *36*, 681–685.
(39) $BiBr_3$: Benda, H. *Z. Kristallogr.* **1980**, *151*, 271–285.
(40) SF_4: (a) Kimura, K.; Bauer, S. H. *J. Chem. Phys.* **1963**, *39*, 3172–3178. (b) Tolles, W. M.; Gwinn, W. D. *J. Chem. Phys.* **1962**, *36*, 1119–1121.
(41) SeF_4: (a) Bowen, H. J. M. *Nature* **1953**, 171. (b) Bowater, I. C.; Brown, R. D.; Burden, F. R. *J. Mol. Spectrosc.* **1968**, *28*, 454–460. (c) Kniep, R.; Poll, W. *Z. Kristallogr.* **1985**, *170*, 101–102.
(42) $SeCl_4$: Kniep, R.; Korte, L.; Mootz, D. *Z. Naturforsch.* **1981**, *36B*, 1660–1662.
(43) $SeBr_4$: Born, P.; Kniep, R.; Mootz, D. *Z. Anorg. Allg. Chem.* **1979**, *451*, 12–24.
(44) TeF_4: Edwards, A. J.; Hewaidy, F. I. *J. Chem. Soc. A* **1968**, 2977–2980.
(45) $TeCl_4$: (a) Buss, B.; Krebs, B. *Angew. Chem., Int. Ed. Engl.* **1970**, *9*, 463. (b) Buss, B.; Krebs, B. *Inorg. Chem.* **1971**, *10*, 2795–2800.
(46) TeI_4: (a) Krebs, B.; Paulat, V. *Angew. Chem., Int. Ed. Engl.* **1976**, *15*, 39–40. (b) Kniep, R.; Beister, H. J.; Wald, D. *Z. Naturforsch.* **1988**, *43B*, 966–980. (c) Krebs, B.; Paulat, V. *Acta Crystallogr.* **1976**, *32B*, 1470–1476.
(47) ClF_5: Altman, A. B.; Myakshin, I. N.; Sukhoverkhov, V. F.; Romanov, G. V.; Spiridonov, V. P. *Dokl. Akad. Nauk SSSR* **1978**, *241*, 360–363.
(48) BrF_5: (a) Burbank, R. D.; Bensey, F. N., Jr. *J. Chem. Phys.* **1957**, *27*, 982–983. (b) Hennan, R. K.; Robiette, A. G. *J. Mol. Struct.* **1979**, *54*, 135–144.
(49) IF_5: (a) Burbank, R. D.; Jones, G. R. *Inorg. Chem.* **1974**, *13*, 1071–1074. (b) Heenan, R. K.; Robiette, A. G. *J. Mol. Struct.* **1979**, *55*, 191–197.
(50) TlF: Alcock, N. W.; Jenkins, H. D. B. *J. Chem. Soc., Dalton Trans.* **1974**, 1907–1911.
(51) InCl: van der Vorst, C. P. J. M.; Verschoor, G. C.; Maaskant, W. J. A. *Acta Crystallogr.* **1978**, *34B*, 3333–3335.
(52) Ng, S.-W.; Zuckerman, J. J. *Adv. Inorg. Radiochem.* **1985**, *29*, 297–323.
(53) (a) Bartell, L. S. *J. Chem. Educ.* **1968**, *45*, 754–767. (b) Burdett, J. K.; Coddens, B. A.; Kulkarni, G. V. *Inorg. Chem.* **1988**, *27*, 3259–3261. (c) Burdett, J. K.; Lin, J.-H. *Acta Crystallogr.* **1981**, *37B*, 2123–2132. (d) Burdett, J. K. *Adv. Chem. Phys.* **1982**, *49*, 47–113. (e) Gimarc, B. M.; Liebman, J. F.; Kohn, M. *J. Am. Chem. Soc.* **1978**, *100*, 2334–2339. Also refer to Gimarc, B. M. *Molecular Structure and Bonding*; Academic Press: New York, 1979; pp 71, 169. (f) MacDougall, P. J. *Inorg. Chem.* **1986**, *25*, 4400–4404. (g) Couch, D. A.; Wilkins, C. J.; Rossman, G. R.; Gray, H. B. *J. Am. Chem. Soc.* **1970**, *92*, 307–310. (h) Hultgren, R. *Phys. Rev.* **1932**, *40*, 891. (i) Albright, T. A.; Burdett, J. K.; Whangbo, M.-H. *Orbital Interactions in Chemistry*; Wiley: New York, 1985; Chapter 14. (j) Shustorovich, E.; Dobosh, P. A. *J. Am. Chem. Soc.* **1979**, *101*, 4090–4095. (k) Gutsev, G. L.; Klyagina, A. P. *Chem. Phys.* **1983**, *75*, 243–252. (l) Knop, O.; Linden, A.; Vincent, B. R.; Choi, S. C.; Cameron, T. S.; Boyd, R. S. *Can. J. Chem.* **1989**, *67*, 1984–2008. (m) Brown, I. D. *J. Solid State Chem.* **1974**, *11*, 214–233. (n) O.-Fourcade, J.; Ibanez, A.; Jumas, J. C.; Maurin, M.; Lefebvre, I.; Lippens, P.; Lannoo, M.; Allan, G. *J. Solid State Chem.* **1990**, *87*, 366–277. (o) Urch, D. S. *J. Chem. Soc.* **1964**, 5775–5781. (p) Schmiedekamp, A.; Cruickshank, D. W. J.; Skaarup, S.; Pulay, P.; Hargittai, I.; Boggs, J. E. *J. Am. Chem. Soc.* **1979**, *101*, 2002–2010. (q) Lefebvre, I.; Lannoo, M.; Allan, G.; Martinage, L. *Phys. Rev.* **1988**, *38B*, 8593–8601.
(54) Relativistic effects: (a) Pyykko, P. *Chem. Rev.* **1988**, *88*, 563–594. (b) Reference 4g, p 22. (c) Pitzer, K. S. *Acc. Chem. Res.* **1979**, *12*, 271–276. (d) Pyykko, P.; Desclaux, J.-P. *Acc. Chem. Res.* **1979**, *12*, 276–281.

(55) (a) Wolfsberg, M.; Helmholtz, L. *J. Chem. Phys.* **1952**, *20*, 837–843. (b) Hoffmann, R.; Lipscomb, W. N. *Ibid.* **1962**, *36*, 2179–2195. (c) Jordan, T.; Smith, H. W.; Lohr, L. L., Jr.; Lipscomb, W. N. *J. Am. Chem. Soc.* **1963**, *85*, 846–851. (d) Ammeter, J. H.; Burgi, H.-B.; Thibeault, J. C.; Hoffmann, R. *J. Am. Chem. Soc.* **1978**, *100*, 3686–3692. (e) Whangbo, M.-H.; Hoffmann, R.; Woodward, R. B. *Proc. R. Soc. London* **1979**, *366A*, 23–46. (f) Lohr, L. L., Jr.; Pyykko, P. *Chem. Phys. Lett.* **1979**, *62*, 333–338. (g) Hughbanks, T.; Hoffmann, R.; Whangbo, M.-H.; Stewart, K. R.; Eisenstein, O.; Canadell, E. *J. Am. Chem. Soc.* **1982**, *104*, 3876–3879. (h) Canadell, E.; Eisenstein, O. *Inorg. Chem.* **1983**, *22*, 2398–2401. (i) Chadi, D. J.; Cohen, M. L. *Phys. Rev.* **1973**, *8B*, 5747–5753.

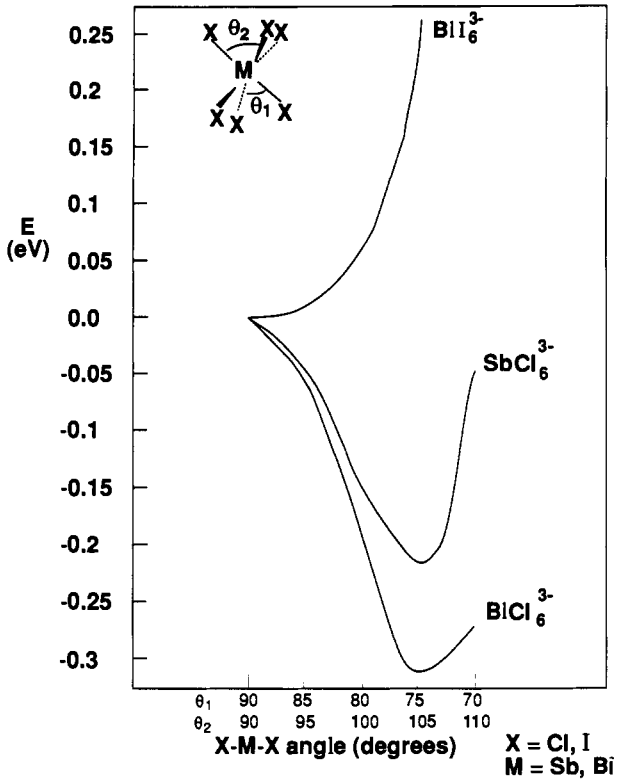

Figure 3. Sums of one-electron energies for $BiCl_6^{3-}$, BiI_6^{3-}, and $SbCl_6^{3-}$ as θ_1 and θ_2 (indicated at top of the figure) are changed from 90° to 70° indicate that only BiI_6^{3-} is more stable in an octahedral structure.

lone pair activity or inactivity in MX_3 solids and MX_6^{3-} molecules based on qualitative symmetry and overlap arguments. Computational and structural details are given in the Appendix.

Bonding in Octahedral and Distorted BiI_6^{3-}

To investigate the nature of the distortion from octahedral to C_{3v} symmetry in molecules of the type MX_6^{3-}, we selected $SbCl_6^{3-}$, $BiCl_6^{3-}$, and BiI_6^{3-} as representatives because they are experimentally known examples of octahedral (BiI_6^{3-}) and distorted octahedral coordination for which the ligands ($BiCl_6^{3-}$) and then the central atom ($SbCl_6^{3-}$) of BiI_6^{3-} have been replaced. We present an interaction diagram for the octahedral BiI_6^{3-} in Figure 2. Although qualitative MO descriptions of bonding in MX_6^{3-} are available,[53a,e,i] we highlight the MOs important for our later discussion. On the left side of Figure 2, the MOs of the I_6^{6-} fragment are shown, and on the right, the orbitals of Bi^{3+} are displayed. The interaction between the orbitals of these two fragments leads to the orbitals of the BiI_6^{3-} molecule, shown in the center of Figure 2. Bi s interacts with two iodine lone pair orbitals to form one bonding, one approximately nonbonding, and one antibonding orbital. The highest energy member of this set is the HOMO of BiI_6^{3-}. It is antibonding between Bi s and hybrids of iodine s and p orbitals. The interaction between Bi p orbitals and iodine lone pairs gives three bonding, three approximately nonbonding, and three antibonding t_{1u} orbitals. The lowest unoccupied MOs of BiI_6^{3-} are the three antibonding partners of the bonding t_{1u}. A single orbital of both the nonbonding and antibonding t_{1u} sets formed from Bi p_z is sketched in Figure 2. The antibonding orbital consists of Bi p_z with a small amount of iodine s and p character. Also sketched in Figure 2 are three iodine lone pair orbitals. Two have strong iodine–iodine antibonding character and no Bi contribution; the third, lowest energy lone pair is weakly iodine–iodine and iodine–bismuth bonding.

Next we calculated the total energy (Figure 3) as the bond angles θ_1 and θ_2 (indicated at the top of Figure 3) are simultaneously varied. For BiI_6^{3-}, the experimentally observed structure with $\theta_1 = \theta_2 = 90°$ is the most stable, lowest energy structure. On the other hand, the C_{3v} structures with $\theta_1 \sim 75°$ and $\theta_2 \sim 105°$ are preferred by 0.3 eV for $BiCl_6^{3-}$ and 0.2 eV for $SbCl_6^{3-}$.

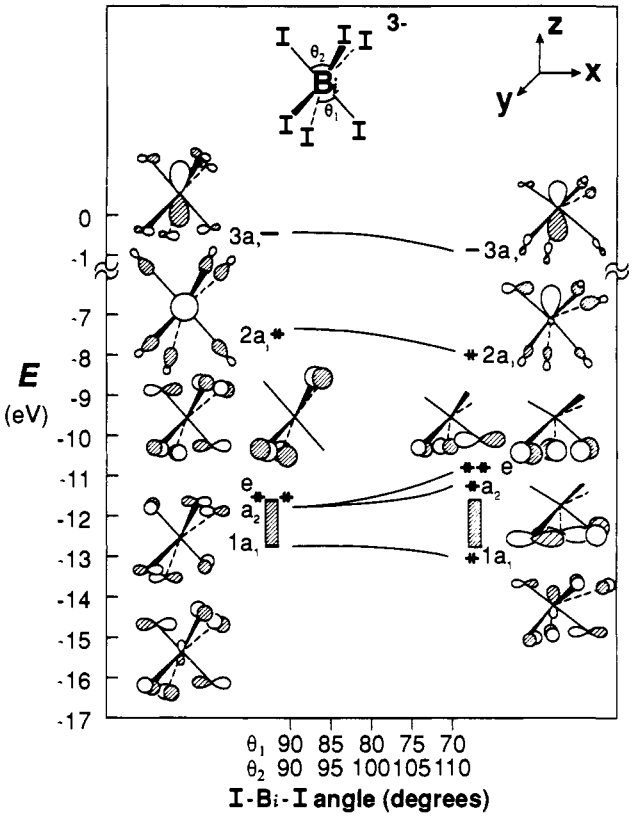

Figure 4. Walsh diagram of orbital energy changes to display the $1a_1$–HOMO mixing and the spreading of the iodine lone pair orbital energies as θ_1 and θ_2 are simultaneously varied for BiI_6^{3-}.

Although the experimentally observed structures for the distorted $BiCl_6^{3-}$ and $SbCl_6^{3-}$ molecules are much closer to 90° and octahedral geometries are also known for both molecules, the experimental structures agree with our finding that distortion from octahedral coordination is easier for $BiCl_6^{3-}$ and $SbCl_6^{3-}$ than for BiI_6^{3-}.

The changes in total energy upon distortion of BiI^{63-} are displayed as individual orbital energy changes in the Walsh diagram of Figure 4. Selected MOs of the octahedral structure are given on the left of Figure 4, and the corresponding MOs of the distorted geometry are shown on the right. The octahedral structure has all I–Bi–I angles equal, and the distorted C_{3v} geometry has three small (θ_1) and three large (θ_2) I–Bi–I angles. At the octahedral geometry both the HOMO and LUMO are Bi–I antibonding.

Upon distortion from octahedral geometry, several important changes take place among the orbitals of octahedral BiI_6^{3-}. The HOMO and the LUMO both decrease in energy. The HOMO is stabilized by mixing with the LUMO, in a second-order Jahn–Teller distortion.[56] The HOMO–LUMO mixing is illustrated in **5** and serves to decrease the coefficients on the bottom three iodines, hybridize the Bi s toward the top three iodines, and decrease the antibonding interaction between Bi and the top three iodines by redirecting the iodine orbitals. The $1a_1$ orbital also

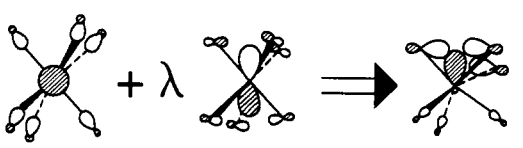

5

mixes with the $2a_1$ HOMO in an antibonding way, to help rehybridize the orbitals on the top three iodines in the HOMO of

(56) Jahn–Teller effect: (a) Bersuker, I. B. *The Jahn–Teller Effect and Vibronic Interactions in Modern Chemistry*; Plenum Press: New York, 1984. (b) Pearson, R. G. *J. Mol. Struct. (THEOCHEM)* **1983**, *103*, 25–34.

Figure 4 and to enhance the directional character of the Bi contribution to the HOMO. The LUMO at the octahedral geometry is mainly composed of Bi p_z. Upon distortion, the HOMO mixes into the LUMO to reduce the contribution from the top three iodines and leave the coefficients of the bottom three iodines in the LUMO more or less unchanged (**6**). The energy decrease

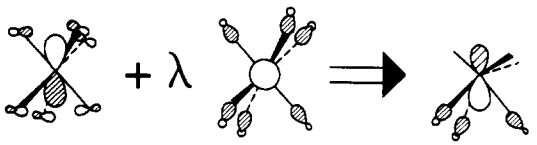

6

of the LUMO can be explained by considering the overlaps of Bi and I orbitals during the distortion. The overlap changes indicate that the antibonding overlap between all iodine AOs and Bi p_z is reduced during the distortion. The small drop in the LUMO energy reflects this decrease in Bi–I antibonding overlap. Both the a_2 and the e orbitals sketched in Figure 4 go up in energy upon distortion from the octahedral geometry. The e orbitals go up in energy by mixing with the lower lying orbitals of the same symmetry. In this process, the contribution from the top three iodines in the e orbitals is nearly canceled. In addition, the lower three iodines in the figure move closer to each other, and their antibonding interaction increases as the value of θ_1 decreases. The a_2 orbital in Figure 4 is pushed up because another low-lying orbital of the same symmetry mixed with it upon distortion from octahedral geometry (**7**). The top three iodine orbital coefficients

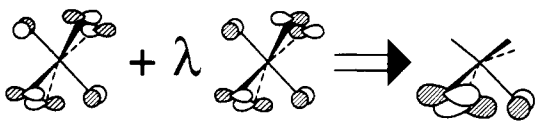

7

on the lower energy a_2 orbital are similar to those in a_2 of Figure 4, but they are opposite in sign. Their mixing cancels the coefficients on the top iodines of a_2 and reinforces the coefficients on the bottom three iodines.

We have performed calculations and generated a Walsh diagram for $BiCl_6^{3-}$ to contrast with Figure 4. We do not present the details, but simply note the following for $BiCl_6^{3-}$ compared to BiI_6^{3-}: (1) the HOMO–LUMO gap is larger, (2) $1a_1$ is further in energy from the HOMO, and (3) the Cl lone pair orbitals spread out much less in energy upon distortion. The smaller HOMO–LUMO gap for BiI_6^{3-} would ordinarily require stronger HOMO–LUMO mixing and a stronger distortion in the case of BiI_6^{3-}. BiI_6^{3-} retains an octahedral geometry whereas $BiCl_6^{3-}$ distorts because $1a_1$ is also much closer to the HOMO in BiI_6^{3-}. $1a_1$ therefore mixes with the HOMO more strongly to keep it at higher energy in BiI_6^{3-}. In addition, the broader block of iodine lone pairs near −12.5 eV on the right side of Figure 4 is a sign of stronger antibonding interactions between iodines than between chlorines, due to the more diffuse orbitals on iodine. This stronger iodine–iodine antibonding interaction is a second factor in the preference of BiI_6^{3-} for an octahedral geometry.

What do the calculations predict for the individual M–X bond lengths? Since the extended Hückel method is well-known to experience difficulties predicting bond lengths, we did not change the M–X distances in our calculations. Table III instead compares the M–X overlap populations, a measure of bond order. In the octahedral geometry, all six M–X overlap populations are equal, but in the distorted geometry, there are two sets of overlap populations: one value, for the bonds defining the larger angle (θ_2), is small, and the second value, for the bonds defining θ_1, is larger. Since the experimental structures for $BiCl_6^{3-}$ and $SbCl_6^{3-}$ show that the shorter bonds bound the smaller angle, θ_1, and the longer bonds define the larger angle, θ_2, experimentally observed bond lengths support our calculated overlap populations. Thus, the calculations imply that the lone pair electrons on the central atom are hybridized toward the longer bonds and larger angles in molecules of the type MX_6^{3-}, M = Bi or Sb; X = I or Cl.

Table III. Calculated Overlap Populations for the Octahedral (O_h) and the C_{3v} Distorted Structures of BiI_6^{3-}, $BiCl_6^{3-}$, and $SbCl_6^{3-}$

		overlap population		
			C_{3v}	
MX_6^{3-}	bond	O_h	θ_1[a]	θ_2[a]
BiI_6^{3-}	Bi–I	0.136	0.206	0.092
$BiCl_6^{3-}$	Bi–Cl	0.049	0.141	−0.002
$SbCl_6^{3-}$	Sb–Cl	0.105	0.210	0.049

[a] $\theta_1 = 70°$ and $\theta_2 = 110°$.

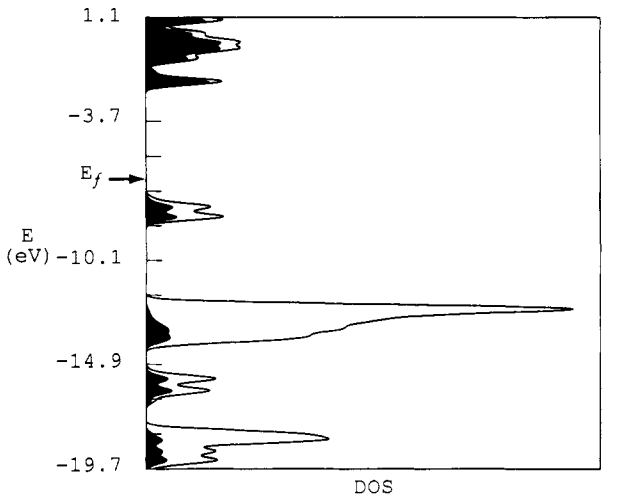

Figure 5. Total density of states (solid line) and density of states (DOS) projection for the bismuth atoms (shaded area) in octahedral BiI_3. E_f indicates the Fermi energy.

The distortion presented in the above discussion hybridizes a lone pair on the central atom toward the face of an octahedron, but we can think of other possible high-symmetry distortions that would direct the central lone pair toward an edge or a vertex of the octahedron. Our calculations show that distortion to hybridize the lone pair toward a face of an octahedron gives a lower energy compared to the other two possible high-symmetry distortions.

The BiI_3 Extended Solid

Since the local coordination geometries of Bi in BiI_3 and of Sb in SbI_3 are similar to the coordination of Bi in the BiI_6^{3-} and $BiCl_6^{3-}$ molecules respectively, we expect many similarities between the electronic structures of the molecular and the solid-state compounds. Figure 5 shows the density of states (DOS) and the projected DOS for the bismuth atoms (shaded area in Figure 5) in BiI_3. The small shaded area in the three lower energy groups of peaks in the projected DOS indicates that the corresponding levels are composed mainly of iodine orbitals. This is because bismuth's share in the total stoichiometry of BiI_3 is only one-fourth and, of this, only the s atomic orbitals have an energy near the iodine s and p levels. The large peak in the middle of Figure 5 contains very little Bi character and can be attributed primarily to the iodine lone pairs. The Bi orbitals are concentrated mainly in the energy levels near 1.1 eV and to some extent in the energy range near −8 eV.

The Bi DOS is further decomposed into s and p_z components in parts a and b of Figure 6. Figure 6a gives the Bi s orbital projection and shows that Bi s is concentrated in the energy ranges immediately above −19.7 eV and near −8 eV. Figure 6b, the projected Bi p_z DOS, shows that the peaks above −3.7 eV contain a large amount of Bi p_z. Bi p_z also makes a small contribution to the predominantly iodine-based levels above −19.7 and −14.9 eV.

The key features highlighted by contrasting parts a and b of Figure 6 are (1) the absence of Bi s character in the energy ranges where Bi p_z appears (above −3.7 eV) and (2) the lack of Bi p_z in the energy range of Bi s. The mutually exclusive Bi s and Bi p_z orbital character in parts a and b of Figure 6 results not from the

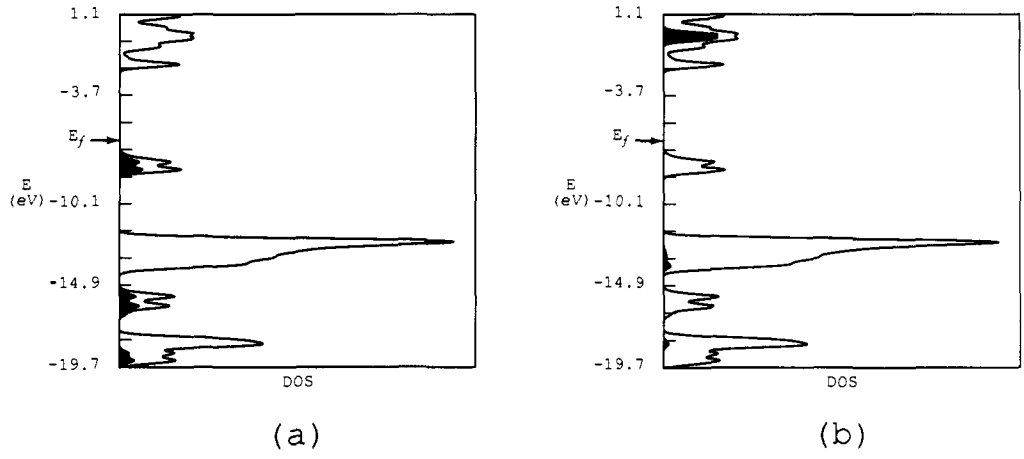

Figure 6. Density of states (DOS) projection (a) for the s orbitals of Bi (darkened area) and (b) for the p_z orbitals of Bi (darkened area) indicate that Bi s and p_z do not mix in BiI_3. The solid line is the total density of states in both a and b. E_f indicates the Fermi energy.

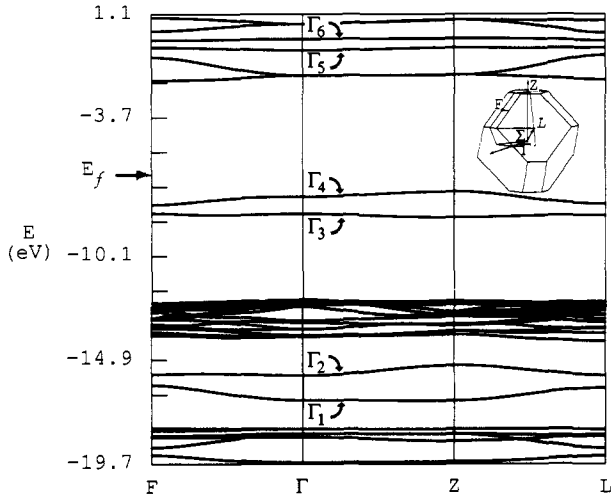

Figure 7. Energy bands of BiI_3. Bands are plotted using the rhombohedral Brillouin zone (inset) along F to Γ to Z to L. E_f indicates the Fermi energy.

space group symmetry of the full BiI_3 structure but from the symmetry of a single "sandwich" consisting of one Bi and two iodine layers. Because the interaction between sandwiches across the van der Waals gap between iodines is very weak, only the symmetry of the individual sandwich is reflected in the orbital mixings. Since the Bi atoms of BiI_3 rest on an inversion center for the isolated sandwich and since s and p_z atomic orbitals have different symmetries under inversion, the mixing of Bi s and p_z is vanishingly small. The most important implications of orbital symmetry will become apparent when we compare the orbitals near the Fermi energy of the distorted SbI_3-type structure with those of BiI_3. But first, we will consider the crystal orbitals of BiI_3 in more detail.

We can investigate the various orbital energy levels and the orbital mixings in detail by considering the individual energy bands for BiI_3. Figure 7 displays the band structure for rhombohedral BiI_3. General features to note include the uniformly flat appearance of most bands, giving rise to the narrow peaks in the density of states curves. The lack of dispersion along the line Γ–Z in the Brillouin zone is expected and confirms that orbital overlap across the van der Waals gap between iodines located in adjacent I–Bi–I sandwiches (stacked along the *c* axis) is very small indeed. Similarly, the iodine lone pair bands just above −14.9 eV are flat throughout the Brillouin zone because of their small mutual overlap and give rise to the large, central peak in the DOS.

The preferred coordination geometry of the Bi atoms is our main focus and can be understood by considering the bonding or antibonding character of specific Bi–I bands. The six lowest energy bands in Figure 7 correspond to the set of peaks near −19.7 eV in the DOS curve, and the two bands just below −14.9 eV (labeled Γ_1 and Γ_2 at the point Γ) lead to the pair of peaks at the same energy in the DOS. Both Γ_1 (sketched in **8a**) and Γ_2 (**8b**) contain

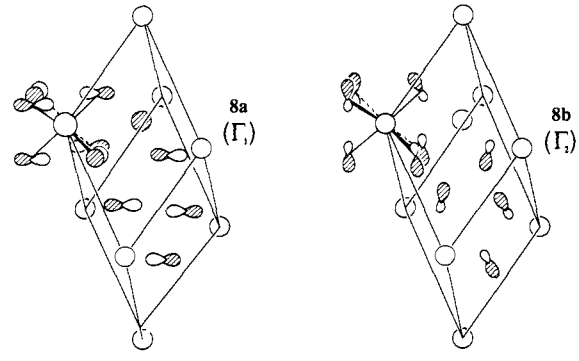

Bi s interacting with I p orbitals in a bonding way. Γ_1 is more bonding than Γ_2 because in Γ_2 the s on I mixes in an antibonding fashion with the Bi s. This mixing reduces the Bi–I bonding interactions and pushes Γ_2 higher in energy than Γ_1. Just above the iodine lone pair orbitals are the two highest occupied crystal orbitals of BiI_3, labeled Γ_3 and Γ_4 and sketched in **8c** and **8d**. Γ_3

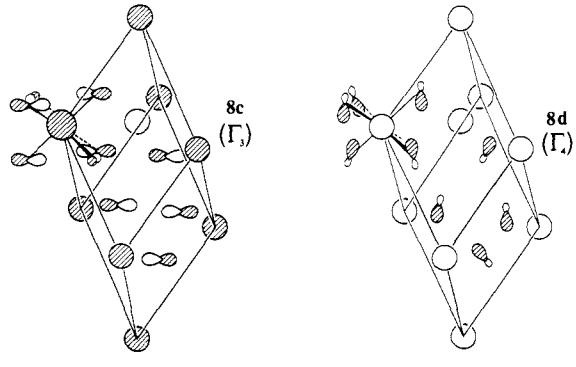

and Γ_4 are the Bi–I antibonding counterparts of Γ_1 and Γ_2 and are thus formed from Bi s and I p orbitals interacting in an antibonding way. Γ_4 is more antibonding than Γ_3 because the iodine orbitals are directed along the Bi–I bonds and the s on the iodines interacts in an antibonding way with the Bi s. Two other important orbitals, Γ_5 and Γ_6, are shown in **8e** and **8f** and are based mainly on Bi p_z. They are unoccupied, and they are antibonding between Bi p_z and iodine p. The Bi s character of Γ_3 and Γ_4, as well as the large Bi p_z contribution to Γ_5 and Γ_6, is consistent with the projected densities of states for Bi s (Figure 6a) and Bi p_z (Figure 6b). The separation of Bi s and p_z orbitals will prove important later, when we consider the distorted structure of SbI_3.

To contrast Bi–I bonding and the character of the lone pair on the central atom in the BiI_3 and SbI_3 structure types, we

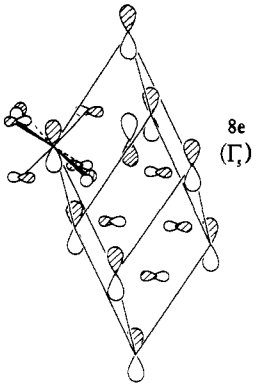

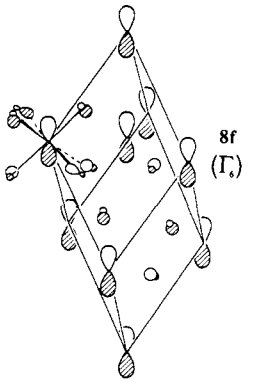

performed band structure calculations for BiI_3 using Bi atoms located at the fractional coordinates for Sb in the SbI_3 structure, and leaving the I atoms at their locations in BiI_3. As a result, the Bi atoms are moved along the 3-fold axis toward one layer of iodines and away from the second layer. The distortion from the BiI_3 structure to a model for the SbI_3 structure type thus gives two sets of three Bi–I distances, one short (2.90 Å) and one long (3.27 Å), and maintains the same space group. Figure 8a shows the total density of states and the Bi s projected density of states for BiI_3 in the SbI_3 structure type. (Although we have plotted the total bismuth DOS projection, it differs little from the bismuth DOS for BiI_3, Figure 5, and we do not show it here.) The most important feature of Figure 8a is the small but significant contribution of Bi s to the highest energy peaks in the DOS.

The contribution of Bi p_z orbitals to the total DOS is displayed in Figure 8b. Bi p_z makes a small contribution to the lowest energy group of peaks as well as to the large peak comprising the iodine lone pairs. Most importantly, a small amount of Bi p_z is mixed into the highest energy occupied bands, bands with a large Bi s component, located just below the Fermi energy. Figure 8b also shows that most of the Bi p_z character spreads into a double peak near 0.0 eV upon distortion.

Again, the various peaks in the DOS can be traced to bands in the band structure plot, Figure 9. For example, the lowest energy peaks in the DOS arise from the six lowest bands in Figure 9, and the peaks just below −14.9 eV are obtained from the two bands appearing near that energy in Figure 9. These two bands are labeled Γ_1' and Γ_2' and are sketched in **9a** and **9b**. Γ_1' and

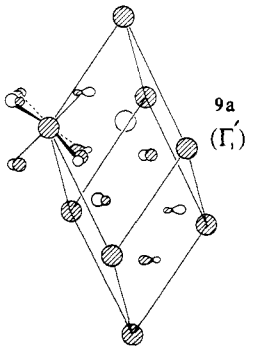

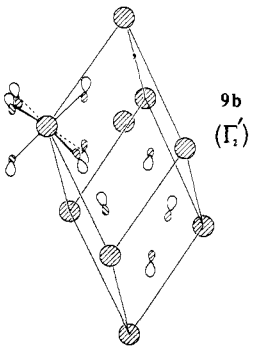

Γ_2' are both Bi–I bonding between Bi s and I p orbitals, but the mixture of I s in Γ_2' serves to hybridize the orbital away from Bi and reduces the bonding interaction. The pair of bands immediately below the Fermi energy are Bi–I antibonding and are sketched in **9c** and **9d**. **9c** (Γ_3') and **9d** (Γ_4') show that these orbitals are formed mainly from Bi s with some Bi p_z mixed in. In Γ_3', the Bi contribution mixes with iodine p in an antibonding way; in Γ_4', Bi orbitals overlap with both iodine s and iodine p in an antibonding way. The orbital composition of these two bands is entirely consistent with the mixing between Bi s and Bi p_z indicated in the projected DOS of Figure 8. Likewise, parts a and b of Figure 8 indicate that a significant amount of Bi p_z is mixed with some Bi s in the highest energy peaks of the DOS plots. These peaks can be traced to Γ_5' and Γ_6', sketched in **9e** and **9f**.

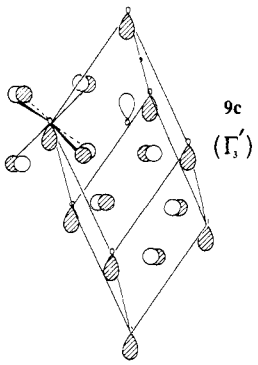

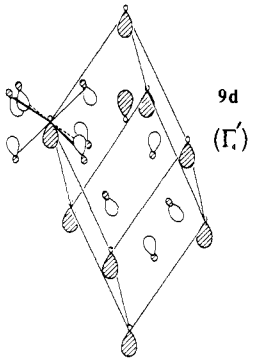

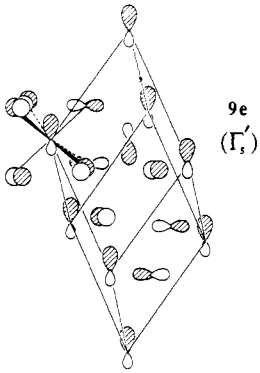

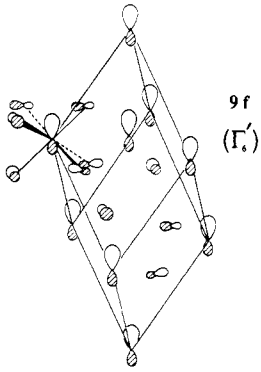

Γ_5' and Γ_6' are antibonding between iodine p and both Bi p_z and Bi s.

Now that we understand the orbitals of BiI_3 and of the model for the SbI_3 structure type, we can contrast the orbitals of the two structures to discover the reasons for the distortion in SbI_3. First, we note that the calculated average energy for BiI_3 in the SbI_3 structure type is nearly 1.3 eV lower than the energy of BiI_3. Since this would suggest that BiI_3 prefers the distorted structure, we repeated the two calculations for Sb instead of Bi and found the distorted structure is favored by more than 6 eV. Hence, the relative energies for BiI_3 in the two structures are not correct, but our calculations show that Bi prefers octahedral coordination in these structures much more than Sb does. We believe, therefore, that the difficulty with total energies reflects the extended Hückel method's well-known deficiency in predicting bond lengths and that the orbitals indeed show the primary interactions responsible for the distortion.

Comparing the projected density of states curves for Bi s and Bi p_z in the BiI_3 structure (parts a and b of Figure 6) with the same projections for BiI_3 in the SbI_3 model structure (parts a and b of Figure 8) gives the major cause of the distortion observed for SbI_3: the mixing of Bi s and Bi p_z levels. The mixing is clearly seen by contrasting the shape of the orbitals **8c** and **8d** for BiI_3 (only s and no p_z on Bi) with **9c** and **9d** for the SbI_3 model structure (p_z mixed with s on Bi). Similarly, **8e** and **8f** (only p_z and no s on Bi) and **9e** and **9f** (s mixed with p_z on Bi) support this picture. In fact, the mixing between the pairs of bands Γ_3 and Γ_4 with Γ_5 and Γ_6 upon distortion occurs not just at Γ but throughout the entire Brillouin zone. Since the levels which combine are nondegenerate, this is similar to a second-order Jahn–Teller distortion and is exactly analogous to the distortion discussed for the MX_6^{3-} molecules.

Conclusions

We have presented simple frontier orbital arguments to provide a unified picture of the "inert pair effect" in the molecules BiI_6^{3-} and $BiCl_6^{3-}$ *and* the extended solids BiI_3 and SbI_3. Extended Hückel molecular orbital calculations show that these compounds tend to exhibit a second-order Jahn–Teller distortion from octahedral to trigonal coordination. The result of the distortion is similar for the molecular and solid-state structures: stereochemically *inactive* lone pair electrons in the highest occupied orbitals of the octahedral structures (BiI_6^{3-} and BiI_3) occupy a spherically

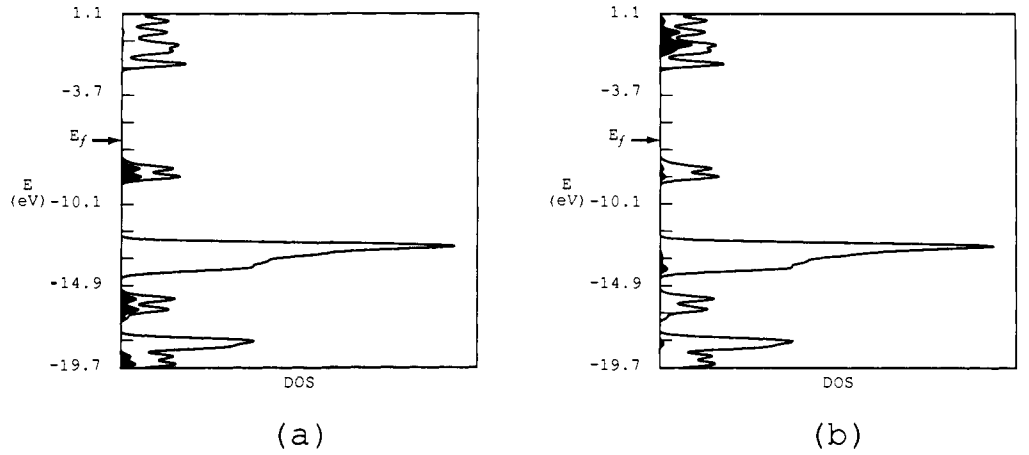

Figure 8. Density of states (DOS) projection (a) for the s orbitals of Bi (shaded area) and (b) for the p_z orbitals of Bi (darkened) show that Bi s and p_z mix in the distorted BiI_3 (SbI_3) structure type.

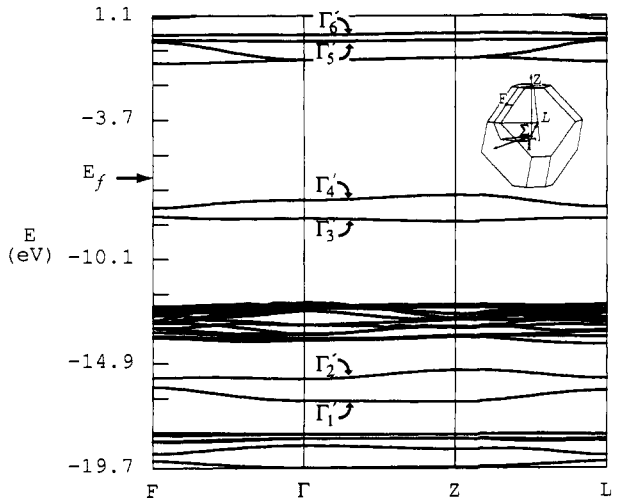

Figure 9. Energy bands of BiI_3 in the SbI_3 structure type. Bands are plotted using the rhombohedral Brillouin zone (inset) along F to Γ to Z to L. E_f indicates the Fermi energy.

Table IV. Parameters Used in the Extended Hückel Calculations

atom	orbital	H_{ii} (eV)	ζ^a	ref
Bi	6s	−15.19	2.56	55f
	6p	−7.79	2.07	
Sb	5s	−18.80	2.32	55g
	5p	−11.70	1.99	
I	5s	−18.00	2.68	55h
	5p	−12.70	2.32	
Cl	3s	−30.00	2.03	
	3p	−15.00	2.03	

[a] Slater exponents.

symmetric Bi s orbital which becomes, upon distortion to the $BiCl_6^{3-}$ or SbI_3 structure types, a stereochemically *active* hybrid of s and p_z. In both cases the hybridization is toward the longer bonds. We infer this from the smaller Bi–I overlap populations along bonds in the direction of the hybrid for the MX_6^{3-} molecules, and we demonstrate it directly in BiI_3 by moving the Bi atoms and noting that the hybrid points toward the longer Bi–I bonds. For the molecules studied, the lone pair is hybridized toward the nominally larger angles; for the MX_3 solids, the lone pair is hybridized toward the *smaller* angles. Thus, the fundamental assumption of VSEPR, i.e., that lone pair electrons demand angular space around the central atom, is confounded in the solid state, and bond length rather than bond angle variations indicate the orientations of lone pair electrons in these compounds.

Whether or not the distortion is structurally realized and the lone pair electrons on the central atom are rendered stereochemically active in the MX_6^{3-} molecules depends upon the energy gap between the HOMO and an a_1 orbital that has primarily ligand lone pair and central atom p_z character. For electropositive central atoms and electropositive ligands, the small HOMO–$1a_1$ gap tempers the distortion and favors the "inert pair effect". Ligand–ligand repulsions, the determinant of molecular structure according to VSEPR, also act to inhibit the distortion.

Acknowledgment. We are grateful to the University of Oklahoma Department of Chemistry and Biochemistry for supporting this work; to the College of Arts and Sciences for providing time on their VAX 6320 computer; to Professor Dick van der Helm and Dr. Masood Khan for crystallographic assistance; and to the Instructional Services Center staff, especially Margaret Smith, for their skillful rendering of the drawings. R.A.W. thanks the University of Oklahoma Research Council for partial support through a Junior Faculty Summer Research Fellowship.

Appendix

All computations were carried out using the extended Hückel method with weighted H_{ij}'s.[55a-d] Atomic parameters for our calculations have been used previously and are given in Table IV. Bond lengths for the calculations are averages of experimentally determined distances. For the molecular structures, bond lengths are 3.07 Å for Bi–I in BiI_6^{3-},[2h] 2.73 Å for Bi–Cl in $BiCl_6^{3-}$,[2b] and 2.70 Å for Sb–Cl in $SbCl_6^{3-}$.[10a] For the solid-state compounds, geometries were determined from fractional coordinates reported in the experimental X-ray diffraction studies. The k-point sets for density of states calculations were special k-point sets chosen using the procedure of Chadi and Cohen.[55l]